2023 IEEE International Conference on Robotics and Automation (ICRA 2023)
May 29 - June 2, 2023. London, UK

# Loitering and Trajectory Tracking of Suspended Payloads in Cable-Driven Balloons Using UGVs

Julius Wanner[1], Eric Sihite[2], Alireza Ramezani[3]*, Morteza Gharib[2]

***Abstract*— Investigations of unmanned aerial vehicles (UAVs) for planetary exploration and payload manipulation have become a strong focus of research within space robotics. Among possible solutions, balloon-based systems possess merits that make them extremely attractive, such as their simple operation mechanism and endured operation time. However, there are many hurdles to overcome to achieve robust trajectory tracking performance for balloon-based applications. In this work, in order to facilitate the control and versatile use of balloons for near-surface planetary payload manipulation, a novel robotic platform and control strategy featuring the coordinated servoing of multiple unmanned ground vehicles (UGVs) to actuate a cable-driven balloon and the suspended payload is proposed. An earthbound prototype and dynamic model of this system are designed to allow for the investigation of payload trajectory tracking performance using a tailored Model Predictive Controller in simulation and experiment.**

## I. INTRODUCTION

Building on a background of successful balloon usage for exploration and reconnaissance on Earth and Venus [1], a robotic platform that renders the use of balloons possible for near-surface aerial mobility and payload manipulation can facilitate access to extreme extraterrestrial terrains and provide new capabilities for planetary reconnaissance, construction and communication. To this extent, a collaborative project between Caltech's *Center for Autonomous Systems and Technologies (CAST)* and Northeastern University's *SiliconSynapse* Lab is initiated and aims to discuss a novel actuation and control framework to enhance low-altitude balloon control capabilities and increase balloon-system versatility.

Other unmanned aerial vehicles (UAVs) such as gliders, rotorcraft and flapping-wing robots have been proposed [2] and deployed [3] for planetary exploration, but can suffer practical issues such as a lack of flight endurance and limited aerodynamic efficiency in environments with a low atmospheric density [4], [5]. The balloon's simple operation mechanism and endured operation time with minimum energy throughput have thus made it attractive for future planetary missions. Prior studies have for instance highlighted applications of balloons to suspend communication devices [6], [7], deploy payloads in Martian craters [8], and perform atmospheric observation and terrain reconnaissance on Mars, Venus or Titan [9], [10], [11], [12]. For both terrestrial and extraterrestrial applications however, underactuated dynamics of slung payloads and environmental factors such as wind disturbances and changing balloon-atmosphere interactions due to a variable thermal environment [13] make effective trajectory prediction and control of these buoyant structures demanding [2], [14]. For high-altitude balloons, some independent systems to alter altitude and lateral balloon position have hence been suggested previously [15], [16], [17], [18] and for near-ground balloon-payload manipulation, a fixed actuator cable-driven balloon concept to set a predetermined balloon payload position within a bound area for the purpose of terrestrial rescue reconnaissance was put forward [19], [20]. Yet despite these efforts, the development of mobile balloon-payload actuation concepts and active closed-loop control strategies enabling precise three-dimensional payload manipulation remains an open challenge and is a major difficulty to overcome to enable the use of balloon systems for planetary aerial mobility operations.

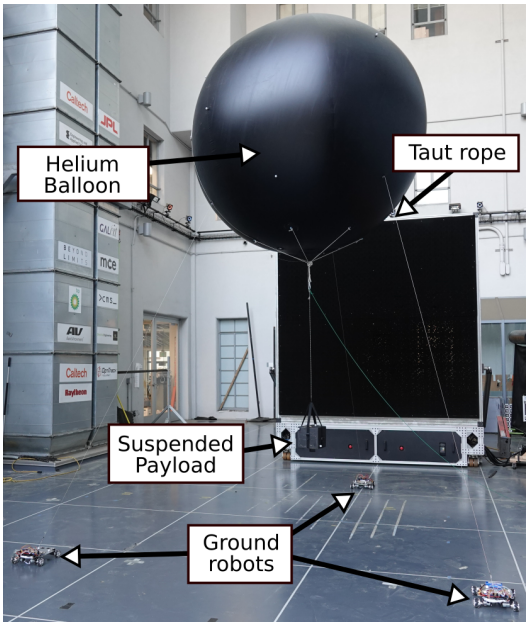


Fig. 1. Novel prototype of a cable-driven balloon with an underactuated hanging payload actuated by the coordinated servoing of multiple UGVs

In response to this problem, considering a focus on near-ground balloon usage for future planetary applications such as scientific exploration, construction or mobile communication stations, in this work it is first proposed to increase

[1] The author is a visiting researcher at the Graduate Aerospace Laboratories of the California Institute of Technology (Caltech GALCIT), Pasadena, CA-91125, USA and with the Department of Mechanical and Process Engineering, ETH Zurich, CH-8092 Zürich, Switzerland. Email: jwanner@student.ethz.ch

[2]The authors are with the Graduate Aerospace Laboratories of the California Institute of Technology (Caltech GALCIT), Pasadena, CA-91125, USA. Emails: esihite, mgharib@caltech.edu

[3] The author is with the SiliconSynapse Laboratory, Department of Electrical and Computer Engineering, Northeastern University, Boston, MA-02119,USA. Email: a.ramezani@northeastern.edu

* This author is the corresponding author.

the action-radius and versatility of a cable-driven balloon system by newly utilizing omnidirectional ground vehicles tethered to a balloon to indirectly regulate the motion of a suspended, underactuated payload. An earthbound prototype of this actuation framework is presented. To achieve closed-loop trajectory control for such a system, given difficulties in obtaining experimental data in extraterrestrial environments it is suggested to pursue model-based control paradigms which can be readily adapted to a variety of system configurations and environments. Reasonable models of the system dynamics can be developed for this purpose and may be extended by available complex balloon-atmosphere interaction models and wind prediction methodologies [21], [22], [23], [24] going forward. In the following, it is commenced by deriving a nonlinear dynamic model of the proposed prototype framework without thermal effects for an arbitrary number of ground vehicle actuators. A tailored Model Predictive Controller (MPC) is consequently designed to determine optimal actuator inputs for smooth and precise tracking of the suspended payload trajectory. The control performance is lastly investigated in simulation and experiments with a Real-Time control architecture provide first validation results.

## II. System Overview

The prototype of the proposed robotic system shown in Fig. 1 features a balloon with a polyvinyl-chloride membrane and an empty structural mass of $\sim$ 3.6 kg and a diameter of 2.2 m. It is filled with Helium, such that it is capable of lifting a payload mass of up to $\sim$ 2 kg at sea-level. The illustrated payload has a mass of 1 kg throughout testing and is attached vertically beneath the balloon's center. The shown two-part tethering configuration is used in order to reduce unwanted pitch and roll movements of the payload about its tether fixation point. Based on prior reasoning for the use of three actuation points to sufficiently regulate cable-driven balloon position [20], three mecanum-wheel omnidirectional UGVs are chosen to actuate the balloon-payload system using individual tether connections consisting of a thin, fabric string. The UGV-balloon tethers are directly fixed to the balloon surface at an elevation angle of 30° from the equator with equal azimuth angles of 120° between each other. Every ground robot possesses a module that receives wireless control commands in form of serial communication packets from a central control machine and transmits these to an onboard microcontroller. The microcontroller then generates low-level signals that drive the UGV omnidirectional wheels. The central controller is run using *Simulink Desktop Real-Time (SDRT)* software to generate and send control inputs. The use of SDRT permits seamless implementation of simulated control algorithms on robot hardware.

## III. Dynamic Model

In this section, a three-dimensional continuous-time dynamic model for the proposed balloon-payload system with an arbitrary number of $n$ actuating UGVs is discussed. The highly-nonlinear equations of motion are derived and implemented in a MATLAB and Simulink simulation framework.

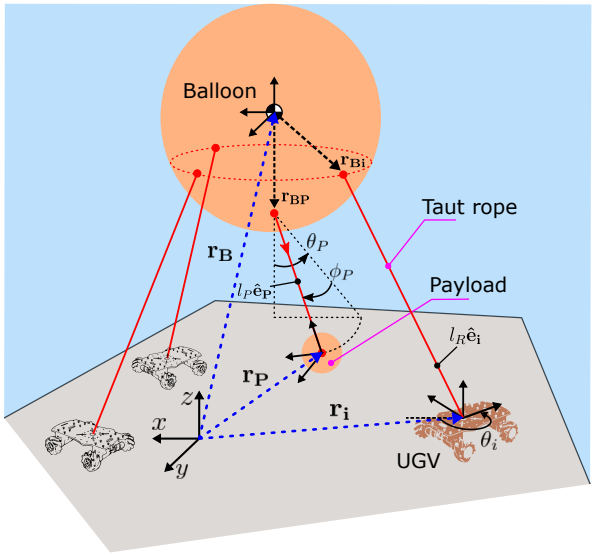


Fig. 2. Model diagram of balloon, payload, and mecanum-wheel UGVs.

The balloon is modeled as a 6-DOF rigid body. The vectors $\mathbf{r_B} = [x_B, y_B, z_B]^\top$ and $\mathbf{\Theta_B} = [\phi_B, \theta_B, \psi_B]^\top$ are chosen to represent the inertial position of the balloon's center of mass and attitude Euler angles, respectively. The tethered payload is assumed as a point-mass single pendulum, where its motion relative to the balloon is described with two coordinates $\mathbf{\Theta_P} = [\phi_P, \theta_P]^\top$ and the payload position in the inertial reference frame is denoted by $\mathbf{r_P} = [x_P, y_P, z_P]^\top$. The above coordinates are illustrated in Fig. 2.

To reduce model complexity for controller development, the omni-directional UGVs are constrained to move on a flat ground plane, where each UGV motion is analyzed with a configuration kinematic model (CKM). The CKMs offer a mathematical model that relates the kinematic states of the UGVs to the physically commanded inputs. The UGV center of mass positions $\mathbf{r_i} = [x_i, y_i, z_i]^\top$, $i \in \{1, \ldots, n\}$ as portrayed in Fig. 2 and their heading angle about the z axis, denoted by $\theta_i$, are used for developing each CKM.

Due to the motional constraints imposed by the tethers connecting each of $n$ UGVs to the balloon, the entire system possesses $8 + 2n$ degrees of freedom. As only one tether links the balloon to the pendulum, the payload is furthermore underactuated. The payload and robot tethers have respective constant lengths denoted by $l_P$ and $l_R$ and their respective directions are parameterized by unit vectors $\hat{\mathbf{e}}_\mathbf{P}$ and $\hat{\mathbf{e}}_\mathbf{i}$. The quantities $\mathbf{r_{BP}}$ and $\mathbf{r_{Bi}}$ illustrated in Fig. 2 describe the distance vectors starting from the balloon center of mass and directed towards the payload attachment point and the i-th UGV tether attachment point respectively.

A Newton-Euler approach is employed to first obtain the equations of motion of the isolated balloon system. The upwards directed net buoyancy force acting on the balloon is defined as

$$F_{B,z} = (\rho_a - \rho_g) V_B g - m_B g \tag{1}$$

for a balloon of structural mass $m_B$ with internal gas volume $V_B$, where $g$, $\rho_a$ and $\rho_g$ denote the gravitational acceleration,

atmospheric density and density of the gas contained in the balloon, respectively. The remaining external forces acting on the balloon are the aerodynamic drag force vector, $\mathbf{F_{D,B}}$, the pendulum (payload) tether tension force vector, $\mathbf{T_p}$, and the tether tension force vector between the balloon and the i-th UGV, $\mathbf{T_i}$. Each tether force vector can only act in the direction of the corresponding tether and is parameterized based on its magnitude and direction, as shown in (2). Note that while complex elastic tether models could be used, with presently minimal tension forces it is chosen to represent the tether connections as inelastic and massless strings that can only support tensile forces.

For a balloon with body-fixed moment of inertia tensor $\underline{I_B}$, the translational dynamics in the inertial frame and rotational dynamics in balloon-body frame are consequently obtained as follows:

$$\begin{aligned} m'_B\ddot{\mathbf{r}}_\mathbf{B} &= \mathbf{F_{D,B}}(\dot{\mathbf{r}}_\mathbf{B}, \mathbf{v_w}) + \mathbf{T_P} + \sum_{i=1}^{n} \mathbf{T_i} \; + \mathbf{W}' \\ \underline{I_B}\dot{\omega}^\mathbf{b}_\mathbf{B} + \omega^\mathbf{b}_\mathbf{B} \times \underline{I_B}\omega^\mathbf{b}_\mathbf{B} &= \mathbf{M^b_P} + \sum_{i=1}^{n} \mathbf{M^b_i} \\ \mathbf{T_P} = \|\mathbf{T_P}\|\hat{\mathbf{e}}_\mathbf{P}, &\qquad \mathbf{M^b_P} = (\mathbf{r^b_{BP}} \times \underline{R_{0b}}\mathbf{T_P}), \\ \mathbf{T_i} = \|\mathbf{T_i}\|\hat{\mathbf{e}}_\mathbf{i}, &\qquad \mathbf{M^b_i} = (\mathbf{r^b_{Bi}} \times \underline{R_{0b}}\mathbf{T_i}) \end{aligned} \tag{2}$$

where $\mathbf{W}' = [0, 0, F_{B,z}]^\top$ and an added mass arising from the air mass that is moved along with the balloon [10] is included in the term $m'_B$. The drag model can furthermore include the effects of an external wind disturbance vector $\mathbf{v_w}$. The superscript $(.)^b$ denotes a quantity in balloon body-fixed frame and the symbols $\|.\|$ and $\times$ signify the Euclidean norm and the vector cross-product, respectively. The angular velocity $\omega^\mathbf{b}_\mathbf{B}$ is used to define the roll, pitch and yaw rates in body-fixed frame. The homogeneous transformation matrix $\underline{R_{0b}} \in \mathbb{R}^{3\times3}$ used in (2) transforms the tether forces and moments from the inertial system into the body frame.

To identify the dynamics of the payload, in the following procedure explicit equations for the angular accelerations $\ddot{\mathbf{\Theta}}_\mathbf{P} = [\ddot{\phi}_P, \ddot{\theta}_P]$ and the tether tension force magnitude $\|\mathbf{T_P}\|$ are derived. First, in (3) the payload position in the inertial frame ($\mathbf{r_P}$) is expressed using geometric relations known from the balloon model. Here, the unit vector $\hat{\mathbf{e}}_\mathbf{P}$ is expressed solely as a function of the payload coordinates $\mathbf{\Theta_P}$, whereas all other quantities are dependent only on the balloon coordinates $\mathbf{r_B}$ and $\mathbf{\Theta_B}$. The first and second order derivatives of (3) are consequently formed to yield expressions for $\dot{\mathbf{r}}_\mathbf{p}$ and $\ddot{\mathbf{r}}_\mathbf{p}$. The three-dimensional equations of motion of the payload in the inertial system are formulated and presented in (4) , where $\mathbf{F_{D,P}}$ represents the aerodynamic drag acting on the payload alone and $\mathbf{W_P}$ is the pendulum weight vector.

$$\mathbf{r_P} = \mathbf{r_B} + \underline{R_{0b}}^\top \mathbf{r^b_{BP}} + l_P\hat{\mathbf{e}}_\mathbf{P} \tag{3}$$

$$m_P\ddot{\mathbf{r}}_\mathbf{P} = \mathbf{F_{D,P}}(\dot{\mathbf{r}}_\mathbf{P}, \mathbf{v_w}) - \mathbf{T_P} - \mathbf{W_P} \tag{4}$$

Next, the introduced expression for $\mathbf{T_P}$ in (2) and the quantities $\mathbf{r_P}$, $\dot{\mathbf{r}}_\mathbf{p}$ and $\ddot{\mathbf{r}}_\mathbf{p}$ obtained in previous steps are substituted into (4). After further substitution of the quantities $\ddot{\mathbf{\Theta}}_\mathbf{B}$ and $\ddot{\mathbf{r}}_\mathbf{B}$ solved in (2), the result is rearranged for the three payload variables $\ddot{\phi}_P, \ddot{\theta}_P, \|\mathbf{T_P}\|$. The combined balloon-payload dynamics are obtained and are given by

$$\begin{aligned} \mathbf{x_{BP}}(t) &= [\,\mathbf{r_B}^\top, \mathbf{\Theta_B}^\top, \mathbf{\Theta_P}^\top, \dot{\mathbf{r}}^\top_\mathbf{B}, \dot{\mathbf{\Theta}}^\top_\mathbf{B}, \dot{\mathbf{\Theta}}^\top_\mathbf{P}\,]^\top \\ \dot{\mathbf{x}}_\mathbf{BP}(t) &= f(\mathbf{x_{BP}}(t), \mathbf{T_i}, \mathbf{v_w}) \end{aligned} \tag{5}$$

where the nonlinear function $f(\mathbf{x_{BP}}(t), \mathbf{T_i}, \mathbf{v_w})$ describes the evolution of the state vector $\mathbf{x_{BP}(t)}$.

### A. UGV Configuration Kinematics Model (CKM)

The selected UGVs use mecanum wheels (also referred to as Swedish wheels) to facilitate omni-directional motion. As the robots are modeled using a CKM formulation, the inputs for the purpose of higher level control are chosen to be the second time derivative of planar position and heading angles of the UGVs. The control inputs of the i-th UGV are thus denoted by $\mathbf{u_i} = [u_{i_1}, u_{i_2}, u_{i_3}]^\top$, where $u_{i,1}$,$u_{i,2}$ and $u_{i,3}$ command the respective rover accelerations $\ddot{x}_i$, $\ddot{y}_i$ and $\ddot{\theta}_i$ in the inertial reference frame.

Though this input structure can be implemented in simulation, in the physical system the input accelerations $\mathbf{u_i}$ cannot be directly actuated. The four mecanum-wheel speeds of every UGV can however be independently controlled on a lower-level such that the commanded accelerations are achieved. The CKM is hence formulated to not only derive the kinematic states of the UGVs in the inertial frame, but to further obtain a set of four wheel angular velocity references for each UGV. These can be derived from the forward kinematics of mecanum-wheel rovers obtained in other work [25]. The CKM formulation relating the acceleration inputs $\mathbf{u_i}$ to the kinematic states and the wheel angular velocities of the i-th UGV is in summary given by:

$$\begin{aligned} \mathbf{x_{R,i}}(t) &= [x_i, y_i, \theta_i, \dot{x}_i, \dot{y}_i, \dot{\theta}_i]^\top \\ \dot{\mathbf{x}}_\mathbf{R,i}(t) &= [\dot{x}_i, \dot{y}_i, \dot{\theta}_i, u_{i_1}, u_{i_2}, u_{i_3}]^\top \\ \mathbf{v_i^R} = \underline{R_{0i}}(\theta_i)[\dot{x}_i, \dot{y}_i]^\top, &\qquad \omega^\mathbf{i}_\mathbf{w} = \underline{T_{kin}}[\mathbf{v_i^R}^\top, \dot{\theta}_i]^\top \end{aligned} \tag{6}$$

where $\mathbf{x_{R,i}}(t)$ denotes the kinematic states used for simulation in the inertial frame, the column vector $\omega^\mathbf{i}_\mathbf{w}$ denotes the four mecanum-wheel angular velocities of the i-th UGV and $\mathbf{v_i^R}$ is the planar velocity vector in the i-th UGV body frame. The matrices $\underline{R_{0i}} \in \mathbb{R}^{2\times2}$ and $\underline{T_{kin}} \in \mathbb{R}^{4\times3}$ respectively denote a 2D planar rotation matrix transforming into body frame and the forward kinematics transformation [25]. In (6), it is assumed that the center of gravity coincides with the robot's geometric center.

### B. Tether Force Constraints

In reality, in addition to being underactuated, the tether tension forces yield switching dynamics. These are overlooked in the following by enforcing a set of constraints when resolving control actions. The magnitudes of the balloon-UGV tension forces $\|\mathbf{T_i}\|$ are obtainable from forward kinematics by assuming the tethers always remain taut, hence through enforcing that each distance vector between the two tether ends, denoted by $\mathbf{\Delta r_i}$, has a magnitude that is always constant and equal to the tether length. This purely state dependent distance constraint is expressed

with a function $K_i$. After double-differentiation and further state variable substitutions a set of $n$ algebraic equations (constraints) denoted by the functions $k_i,\ i \in \{1,\dots,n\}$, which are implemented in simulation, is obtained. The tether geometric quantities and constraint function expressions are summarized in (7) below,

$$\begin{aligned} \mathbf{\Delta r_i}(\mathbf{x_{BP}}(t), \mathbf{x_{R,i}}(t)) &= \mathbf{r_i} - (\mathbf{r_B} + \underline{R_{0b}}^{\top} \mathbf{r_{Bi}^b}) \\ K_i(\mathbf{x_{BP}}(t), \mathbf{x_{R,i}}(t)) &= \|\mathbf{\Delta r_i}\|^2 = {l_R}^2 \\ k_i(\mathbf{x_{BP}}(t), \mathbf{x_{R,i}}(t), \|\mathbf{T_i}\|, \mathbf{u_i}, \mathbf{v_w}) &= 0 \end{aligned} \tag{7}$$

where it is assumed for simplicity that the tethers are attached directly to the center of gravity of the robot.

## IV. Robot Control

In this section, an MPC-based approach to achieve closed-loop tracking of desired payload trajectories is described. The control objectives and the constrained finite horizon optimization problem building upon the previously derived dynamic model are formulated in order to determine the optimal control moves. The control architecture utilized for testing in the *Caltech CAST* Arena is highlighted.

### A. Objectives

The system's main functionality is to transport a payload aerially from an initial to a final rest point. The primary control objective is hence to ensure that the payload position $\mathbf{r_P}$ reaches a goal position $\mathbf{r_{P,ref}}$ within a given timeframe. By providing time-varying reference positions to the control system, tracking of predefined waypoints, as could be obtained from a path-planner, can furthermore be achieved. Unfavorable dynamic modes and disturbances, e.g. caused by Martian winds, can however agitate the system and cause oscillations of the payload at rest or during the transport phase. Such oscillations may destabilize the system and decrease the the ability to reliably reach a target position. Therefore, a secondary control reference seeking to minimize the payload swing velocities is set as $\mathbf{\dot{\Theta}_{P,ref}} = [0,0]^{\top}$.

### B. Model Predictive Control Formulation

An optimal control problem over the prediction horizon $T_p$ is formulated as the following:

$$\min_{u(\cdot)} \int_0^{T_p} \Phi_L(t, \mathbf{x}(t), \mathbf{u}(t), \mathbf{d}) dt$$

$$\begin{aligned} \textbf{subject to:}\quad & \mathbf{x}(0) = \mathbf{x_0}, \quad \dot{\mathbf{x}}(t) = \mathbf{f}(t, \mathbf{x}(t), \mathbf{u}(t), \mathbf{d}) \\ & |\mathbf{x}(t)| \le \mathbf{a_x}, \qquad 0 = \mathbf{g}(t, \mathbf{x}(t), \mathbf{u}(t), \mathbf{d}) \\ & |\mathbf{y}(\mathbf{x}(t))| \le \mathbf{a_y}, \quad \mathbf{u_v} \ge 0, \qquad |\mathbf{u_R}| \le \mathbf{a_u} \end{aligned} \tag{8}$$

where the states $\mathbf{x}(t) = [\mathbf{x_{BP}}^{\top}, \mathbf{x_{R,1}}^{\top}, \dots, \mathbf{x_{R,n}}^{\top}]^{\top}$ and outputs $\mathbf{y}(\mathbf{x}(t)) = [\mathbf{r_p}^{\top}, \mathbf{\dot{\Theta}_P}^{\top}]^{\top}$ for the prediction model assume a total of $n$ UGVs. In the constraint equations above, a disturbance term $\mathbf{d} = \mathbf{v_w}$ is included to account for effects of the wind velocity on drag forces. The input vector denoted by $\mathbf{u}(t) = [\mathbf{u_v}(t)^{\top}, \mathbf{u_R}(t)^{\top}]^{\top}$ is composed of inputs to the balloon-payload system in form of the UGV-balloon tether tension forces $\mathbf{u_v}(t) = [|\mathbf{T_1}|, \dots, |\mathbf{T_n}|]^{\top}$ and inputs to UGVs $\mathbf{u_R}(t) = [\mathbf{u_1}^{\top}, \dots, \mathbf{u_n}^{\top}]^{\top}$.

As the control problem mandates positive tension force magnitudes across the prediction horizon, all virtual inputs $\mathbf{u_v}(t)$ are bounded to be greater than or equal to zero. Other feasibility constraints are embodied in the lower and upper bounds for the UGV acceleration inputs ($\mathbf{a_u}$), limits for state variables such as the robot position and robot velocities ($\mathbf{a_x}$) and constraints on the payload position output variables ($\mathbf{a_y}$).

The constrained optimization problem is resolved using MATLAB and Simulink. To reduce the complexity of the MPC state model, it is chosen to implement the UGV-tether tension force magnitudes as the additional inputs $\mathbf{u_v}(t)$. Both inputs $\mathbf{u_v}(t)$ and $\mathbf{u_R}(t)$ are optimized simultaneously whilst being subjected to a set of $n$ nonlinear equality constraint functions $\mathbf{g}$ in (8). Each element of $\mathbf{g}$ represents a constant tether length constraint between the i-th UGV and balloon and is given as $\mathbf{g_i} = K_i(\mathbf{x_{BP}}(t), \mathbf{x_{R,i}}(t)) - {l_R}^2$ based on the definitions in (7). This ensures that the physical relation between the robot accelerations and tether forces is maintained while the computational efforts to resolve the constraints are kept at a minimum.

In (8), the Lagrange term is chosen to minimize the control input variations $\dot{\mathbf{u}}(t)$ over time and to track the output reference given by $\mathbf{r}(t) = [{\mathbf{r_{P,ref}}}^{\top}, \mathbf{\dot{\Theta}_{P,ref}}^{\top}]^{\top}$. It is given as:

$$\begin{aligned} \Phi_L(t, \mathbf{x}(t), \mathbf{u}(t), \mathbf{d}) = & ||\mathbf{c_y} \odot \mathbf{w_y} \odot (\mathbf{r}(t) - \mathbf{y}(\mathbf{x}(t))||^2 \\ & + ||\mathbf{c_u} \odot \mathbf{w_{\Delta u}} \odot \dot{\mathbf{u}}(t)||^2 \end{aligned} \tag{9}$$

where $\mathbf{w_y}, \mathbf{w_{\Delta u}} \in \mathbb{R}^5$ are weight column vectors for the output reference tracking and control input aggressiveness terms, respectively. The column vectors $\mathbf{c_y}, \mathbf{c_u} \in \mathbb{R}^5$ respectively scale output and input variables for optimization and are given as the reciprocals of the respective expected value ranges. The operator $\odot$ denotes element-wise vector multiplication.

### C. Real-Time Control architecture in CAST Arena

In a planetary deployment scenario, the Model Predictive Controller receives a reference signal from a user or a higher-level trajectory planner. It obtains state measurements which can be complemented by internally computed state estimations if the system states are not fully measurable. To simplify controller deployment on the existing prototype in the *Caltech CAST* arena, a camera-based motion capture system is used to provide state measurements and guarantee full system state observability. The controlled variables are the robot accelerations in the inertial reference frame given by $\mathbf{u_i},\ \ i \in \{1,\dots,n\}$ as defined prior. These accelerations are piecewise constant over a control interval and are integrated over the control sample time to provide a velocity change reference signal $\mathbf{\Delta} v_{i,ref}$. In closed loop operation, this reference is summed with the robot initial velocity vector updates $\mathbf{v_{i,0}}$ measured at the beginning of the control interval. Consequently, using the CKM model derived in (6), a set of four wheel rotational speed references $\omega_{\mathbf{w,ref,i}}$ is obtained. These are sampled at a freqeuency of $\sim$ 20 Hz and transmitted wirelessly from the central control unit to every robot. Each robot is driven by an internal PI controller that receives a rotational speed feedback signal

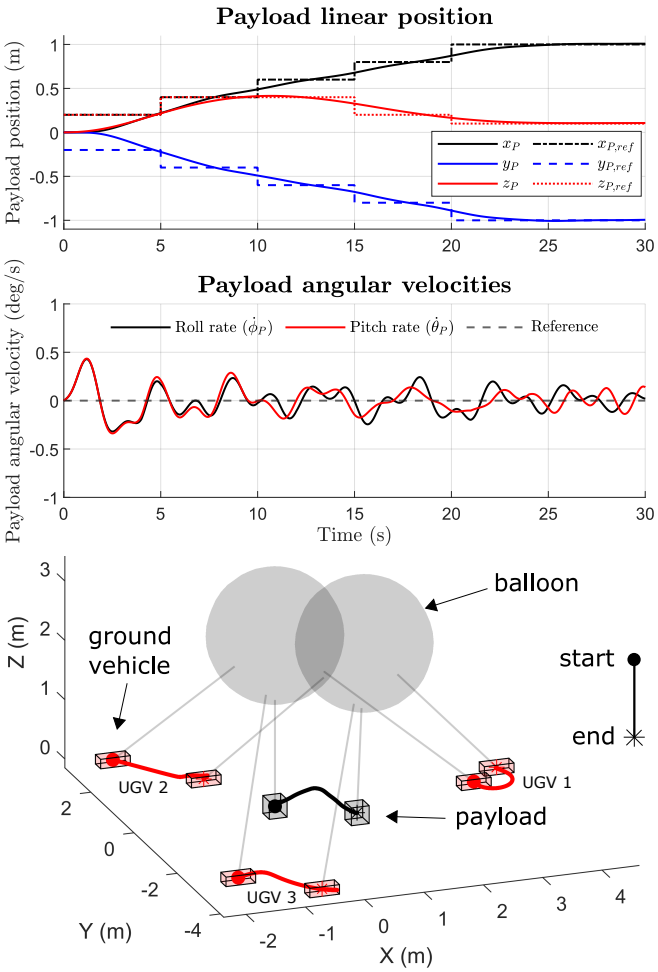


Fig. 3. Simulated payload position trajectories and tether angular velocities for closed-loop tracking of a reference trajectory using LTV-MPC.

from encoders at every wheel and accordingly regulates the motor drive voltage to track the wheel speed references.

## V. Results

In this section, simulation and current experimental results are briefly presented. It is shown that the closed loop system is able to track time-varying reference waypoints for the payload positions whilst ensuring steady-state stability. First measurements from the physical system are gathered to validate the system model and to allow for controller testing.

### A. Simulation

Closed-loop control simulations for the developed plant model actuated by three ground robots ($n = 3$) are performed. The MPC states, output and constraint functions are derived symbolically in continuous time and are converted to a discrete time formulation. Due to the slow dynamics of the system, a control sample time on the order of 1.0 seconds is presently chosen to implement the controller. It was found that the computation time of the nonlinear optimization in simulation using standard sequential quadratic programming solvers however significantly exceeds the control sample time. Thus, a linear time-varying (LTV) model predictive

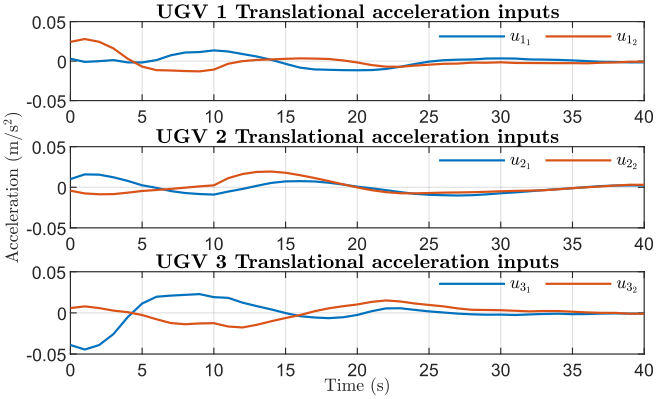


Fig. 4. UGV translational acceleration control actions for closed-loop tracking of a time-varying reference payload trajectory using LTV-MPC

controller is implemented and optimal control solutions are solved using MATLAB MPC Toolbox interior-point solvers. This control framework has proven to greatly reduce the execution time in simulation whilst providing closed-loop results that are comparable to fully nonlinear MPC. Equivalent prediction and control horizons of 15 seconds are chosen. The scaling vectors are defined in order to obtain values of inputs and outputs that are of roughly unit-order for the evaluation of the optimization cost-function (9). Adding to this, the input variation cost weight vector $\mathbf{w_{\Delta u}}$ is chosen to prioritize small changes in the tether tension force magnitudes in order to reduce the likelihood of temporarily losing tension in the tethers. The output weight vector $\mathbf{w_y}$ is biased towards tracking of the payload swing velocities $\dot{\mathbf{\Theta}}_\mathbf{P}$ such that steady-state system stability is achieved.

Throughout simulation, the absolute translational acceleration inputs $u_{i,1}, u_{i,2}$ are conservatively limited to 0.1 $m/s^2$ to avoid excessive wheel-slip in practice. The UGV rotational acceleration inputs $u_{i,3}$ are not actuated in current experiments and therefore remain zero at every time step. A time-varying reference signal imitating a trajectory that could be obtained from a path planner in practical applications is implemented. The reference values are updated every five seconds. In the investigated scenario, the payload is initially at rest on the ground surface with its initial position given as $\mathbf{r_{P,0}} = [0, 0, 0]^\top$. The payload should then be lifted to and briefly hover at a height of 0.4 m, whilst moving uniformly in the positive longitudinal X and negative longitudinal Y directions. The payload is lastly commanded to continue its longitudinal trajectory whilst moving down vertically to a height of 0.1 m to reach a steady state position $\mathbf{r_{P,\infty}} = [1, -1, 0.1]^\top$ after a total time of $\sim$ 25 seconds. The absolute payload swing angle velocities $\dot{\mathbf{\Theta}}_\mathbf{P}$ are to be minimized throughout the transport process and after the final position is reached. To allow for smooth and foresighted tracking of the varying references, the implemented MPC furthermore uses reference previewing. This feature accounts for future reference changes when updating the prediction model and determines a foresighted set of optimal control moves. The reference signal and obtained closed-loop simulation outputs for the described scenario are given in Fig. 3.

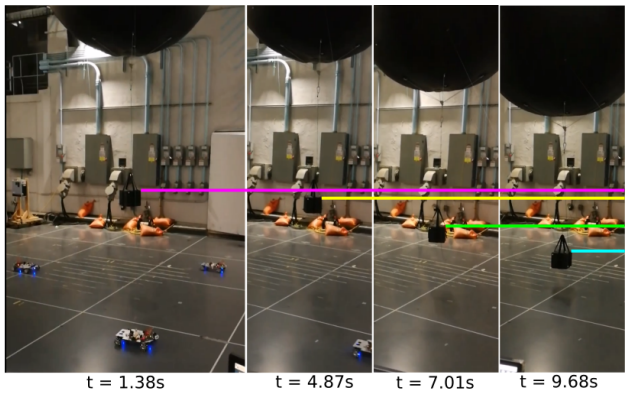


Fig. 5. Snapshots taken during experiment Case 3. Lines indicate the downwards motion of the payload achieved through outwards UGV motions

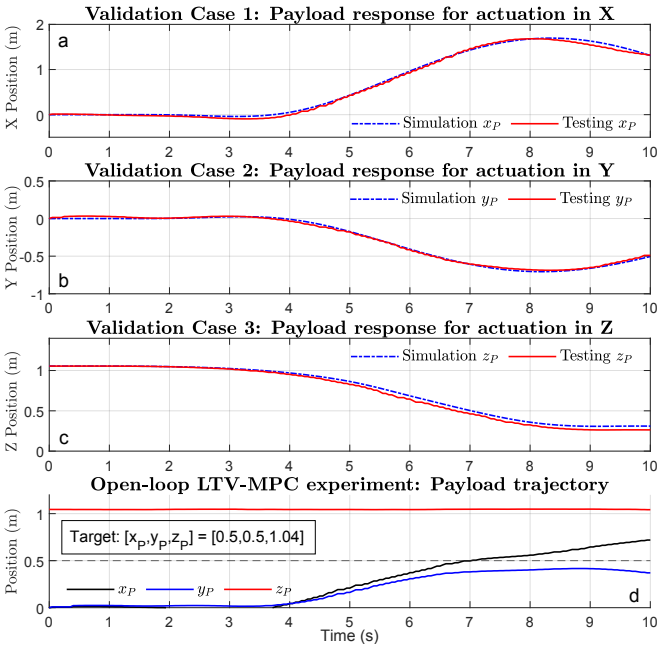


Fig. 6. **(a-c)** Simulated and measured payload responses for actuation in longitudinal, lateral and vertical directions for respective experiments Case 1, Case 2 and Case 3. **(d)** Measured payload position response to step reference with open-Loop LTV-MPC control actions

The corresponding UGV input accelerations shown in Fig. 4 prove to satisfy the imposed input constraints and ensure maintained UGV tether tension.

Additional simulations of the closed-loop response to varying and step position references under the action of a constant unmeasured wind disturbance velocity vector have been conducted and show that the controlled system is stable, but that the steady-state tracking accuracy is reduced. The developed MPC model is however able to consider wind velocities as a measured disturbance, in which case simulation results yield satisfactory tracking accuracy. For a future full-scale system, it is therefore to be considered to include wind speed sensors for control feedback.

### *B. Experiments*

To validate the system model in experiment, the state responses of the prototype to different feed-forward control inputs are measured and compared to simulation results. The three rovers are commanded with predefined velocity profiles constructed from acceleration and deceleration inputs of piece-wise constant and equal magnitude. Three experiment cases are considered: In Case 1, the UGVs are actuated equally only in the longitudinal X-direction, whereas in Case 2, all rovers are equally actuated only in the lateral Y-direction. In Case 3, the payload is to be moved vertically as shown in Fig. 5 by moving the rovers apart longitudinally, that is by providing an X-direction velocity reference to UGV 1 that is equal in magnitude but opposite in direction to that of UGVs 2 and 3. The realized robot velocities in the inertial plane and all remaining system states and outputs are measured using motion capture. Filtered UGV acceleration profiles are derived from the velocity measurements and given as a time-varying input to the simulation model, where the simulated plant output trajectories are extracted. Fig. 6 (a-c) compares the simulated and measured payload outputs, where it is seen that a good agreement between the tested and simulated trajectories in the relevant directions exists for these decoupled cases. First open-loop measurements under the action of precalculated MPC control inputs for a step reference target position are presented in Fig. 6 (d). These indicate the ability of the LTV-MPC to steer the system in the vicinity of the target within a 15 s prediction horizon time despite the lack of state feedback, thereby further validating the controller prediction model. Control software optimization to perform closed-loop experimentation is ongoing.

## VI. CONCLUSIONS

In this work, a novel actuation and control framework to enhance payload manipulation capabilities on the basis of using ground-vehicles to actuate a cable-driven balloon is presented. The development of a terrestrial demonstrator and dynamic model of the robotic system along with the proposal of a Model Predictive Control architecture to achieve loitering and trajectory tracking of an underactuated, balloon-suspended payload has been achieved. In the future, the proposed system can be scaled for planetary exploration applications at low-altitudes ($< 100$ m) such as construction, payload transport and communication. Hurdles in modeling, robust control design and hardware development nonetheless remain to be overcome to achieve full-scale deployment. To this extent, in further work it is targeted to ensure robust trajectory tracking performance against experimentally identified disturbances and uncertainties by exploring robust MPC architectures for nonlinear systems [26], [27]. A dedicated MPC software implementation on a microcontroller can furthermore reduce closed-loop execution time. Improvements of the system model that accommodate thermal effects on the balloon and uneven terrains will additionally allow system simulation for a sample Martian use-case. Besides the otherwise required mechanical system modifications to suit harsh extraterrestrial environments, a revised sensor suite and state estimation architecture that does not rely on motion capture feedback and can consider measurable disturbances is a crucial step towards realizing a full-scale prototype.

## REFERENCES


[1] R. Z. Sagdeev, V. M. Linkin, J. E. Blamont, and R. A. Preston, "The VEGA Venus Balloon Experiment," *Science*, vol. 231, no. 4744, pp. 1407–1408, Mar. 1986.

[2] M. Sharma, A. Gupta, S. K. Gupta, S. H. Alsamhi, and A. V. Shvetsov, "Survey on Unmanned Aerial Vehicle for Mars Exploration: Deployment Use Case," *Drones*, vol. 6, no. 1, p. 4, Dec. 2021.

[3] J. Balaram, M. Aung, and M. P. Golombek, "The Ingenuity Helicopter on the Perseverance Rover," *Space Science Reviews*, vol. 217, no. 4, p. 56, May 2021.

[4] S. A. H. Mohsan, N. Q. H. Othman, Y. Li, M. H. Alsharif, and M. A. Khan, "Unmanned aerial vehicles (UAVs): practical aspects, applications, open challenges, security issues, and future trends," *Intelligent Service Robotics*, Jan. 2023.

[5] E. Giacomini, L.-G. Westerberg, and G. Nikolakopoulos, "A Survey on Drones for Planetary Exploration: Evolution and Challenges," in *2022 30th Mediterranean Conference on Control and Automation (MED)*. Vouliagmeni, Greece: IEEE, Jun. 2022, pp. 583–590.

[6] M. Lally, M. Chamieh, R. Daruwala, V. Duong, H. Hall, S. Holt, L. Nguyen, R. Rafizadeh, P. S. Fah, K. Weng, C. Yuan, T. Bewley, R. Alimo, and C. Derewa, "Tethered Balloon-Based Experiment of Surface Water Height Using Satellite Signals of Opportunity," in *2020 IEEE Aerospace Conference*. Big Sky, MT, USA: IEEE, Mar. 2020, pp. 1–7.

[7] S. A. Khaleefa, S. H. Alsamhi, and N. S. Rajput, "Tethered balloon technology for telecommunication, coverage and path loss," in *2014 IEEE Students' Conference on Electrical, Electronics and Computer Science*. Bhopal: IEEE, Mar. 2014, pp. 1–4.

[8] G. Meirion-Griffith, I. Nesnas, L. Kerber, R. Anderson, T. Brown, F. Calef, J. Burdick, and M. Tanner, "Accessing mars recurring slope lineae: Mobility systems analysis," in *2018 IEEE Aerospace Conference*, Mar. 2018, pp. 1–13.

[9] T. Gamber, K. Nock, J. Balaram, M. Heun, I. Smith, K. Nock, J. Balaram, M. Heun, I. Smith, and T. Gamber, "Mars 2001 Aerobot/Balloon System overview," in *International Balloon Technology Conference*. San Francisco,CA,U.S.A.: American Institute of Aeronautics and Astronautics, Jun. 1997.

[10] K. Garg and T. Kuhn, "Balloon Design for Mars, Venus, and Titan Atmospheres," *Applied Sciences*, vol. 10, no. 9, p. 3204, Jan. 2020.

[11] G. Landis, "Low-Altitude Exploration of the Venus Atmosphere by Balloon," in *48th AIAA Aerospace Sciences Meeting Including the New Horizons Forum and Aerospace Exposition*. Orlando, Florida: American Institute of Aeronautics and Astronautics, Jan. 2010.

[12] M. Anyoji, H. Nagai, and A. Oyama, "Evaluation of Aerodynamic Performance of Mars Airplane in Scientific Balloon Experiment," *Fluid Mechanics Research International Journal*, vol. 1, Nov. 2017.

[13] X.-L. Xia, D.-F. Li, C. Sun, and L.-M. Ruan, "Transient thermal behavior of stratospheric balloons at float conditions," *Advances in Space Research*, vol. 46, no. 9, pp. 1184–1190, Nov. 2010.

[14] L. Renegar, "A Survey of Current Balloon Trajectory Prediction Technology," *Academic High Altitude Conference*, vol. 2017, no. 1, Oct. 2017.

[15] K. T. Nock, K. M. Aaron, M. K. Heun, and A. A. Pankine, "Aerodynamic and Mission Performance of a Winged Balloon Guidance System," *Journal of Aircraft*, vol. 44, no. 6, pp. 1923–1938, Nov. 2007.

[16] C. D. Yoder, S. Agrawal, A. G. Motes, and A. P. Mazzoleni, "Aerodynamic Tethered Sails for Scientific Balloon Trajectory Control: Small-Scale Experimental Demonstration," *Journal of Aircraft*, vol. 58, no. 5, pp. 1010–1021, Sep. 2021.

[17] J. L. Hall, M. Pauken, A. Schutte, S. Krishnamoorthy, C. Aiazzi, J. Izraelevitz, T. Lachenmeier, and C. Turner, "Prototype Development of a Variable Altitude Venus Aerobot," in *AIAA AVIATION 2021 FORUM*. VIRTUAL EVENT: American Institute of Aeronautics and Astronautics, Aug. 2021.

[18] T. Schuler, S. Shkarayev, and J. Thangavelautham, "Altitude Control of a Solar Balloon for Mars Exploration," *Advances in the Astronautical Sciences*, Jan. 2020.

[19] F. Takemura, M. Enomoto, T. Tanaka, K. Denou, Y. Kobayashi, and S. Tadokoro, "Development of the balloon-cable driven robot for information collection from sky and proposal of the search strategy at a major disaster," in *Proceedings, 2005 IEEE/ASME International Conference on Advanced Intelligent Mechatronics.*, Jul. 2005, pp. 658–663.

[20] F. Takemura, K. Maeda, and S. Tadokoro, "Attitude Stability of a Cable Driven Balloon Robot," in *2006 IEEE/RSJ International Conference on Intelligent Robots and Systems*, Beijing, China, 2006, pp. 3504–3509.

[21] X. Yang, W. Zhang, and Z. Hou, "Improved Thermal and Vertical Trajectory Model for Performance Prediction of Stratospheric Balloons," *Journal of Aerospace Engineering*, vol. 28, no. 3, p. 04014075, May 2015.

[22] P. Alexander, "A numerical study of open atmospheric balloon dynamics," *Physics of Fluids*, vol. 15, no. 3065, Sep. 2003.

[23] S. M. Osprey, "Autonomous balloons take flight with artificial intelligence," *Nature*, vol. 588, no. 7836, pp. 33–34, Dec. 2020.

[24] K. Garg, "Wind Based Navigation for Zero-Pressure Stratospheric Balloons Using Reinforcement learning," *Acta Astronomica*, 2019.

[25] H. Taheri, B. Qiao, and N. Ghaeminezhad, "Kinematic Model of a Four Mecanum Wheeled Mobile robot," *International Journal of Computer Applications*, vol. 113, no. 3, Mar. 2015.

[26] M. Rubagotti, D. M. Raimondo, A. Ferrara, and L. Magni, "Robust Model Predictive Control With Integral Sliding Mode in Continuous-Time Sampled-Data Nonlinear Systems," *IEEE Transactions on Automatic Control*, vol. 56, no. 3, pp. 556–570, Mar. 2011.

[27] D. Ji, J. Ren, C. Liu, and Y. Shi, "Stabilizing terminal constraint-free nonlinear MPC via sliding mode-based terminal cost," *Automatica*, vol. 134, p. 109898, Dec. 2021.